



Cite this: DOI: 10.1039/c7dt03734a

Tailoring 2D and 3D molecular sieves structures for polyolefin composites: do all roads lead to remarkable performances?†

H. M. Moura,^a N. L. Gibbons,^{‡b} S. A. Miller ^b and H. O. Pastore ^{*a}

Multiple synthetic strategies were performed in order to tether a zirconium-based catalyst to the 2D and 3D molecular sieves for olefin polymerizations. The anchoring of fluorene silane to the mesoporous MCM-41 was performed in order to obtain a stable catalyst for olefin polymerization (**1**@MCM-41). Using spectroscopic methods, this system was shown to have the metal center locked on a face down conformation with the surface. Also, immobilized zirconium complexes have been prepared on three different types of aminopropyl-modified supports (**2**@magadiite, **2**@MCM-41 and **3**@MCM-48). The advantage of this latter method of immobilization would be the reduction of the steric effect caused by the support: the catalyst, distant from the surface, is more exposed to the monomer and this situation may lead to an increase in the catalytic activity compared to **1**@MCM-41. However, a medium size chain as a spacer between the support and the metallocene is still flexible enough to bend and predisposes the metal center to interact with the support surface; this effect is more evident when the nature of the support is of fixed pore dimensions. These supported catalysts exhibited activity for ethylene polymerization, resulting in linear PEs with high melting temperatures. In order to retain a metallocene assembled as in a homogeneous environment, a multi-step reaction was investigated (**4**@magadiite) but it led to the leaching of the organic moieties from the surface during catalyst preparation. The best catalytic performance was achieved when homogeneous Oct-amido catalyst (**5**) was reacted with the surface of magadiite and *n*-alkyl-AlPO-kan.

Received 4th October 2017,
Accepted 19th December 2017

DOI: 10.1039/c7dt03734a

rsc.li/dalton

1. Introduction

Polyolefins such as polypropylene (PP) and polyethylene (PE) are the largest contributors to the world-scale polymer production.^{1,2} Such polyolefins are currently produced industrially by using metallocene catalysts. Some problems still persist such as the control of the polymer morphology with homogeneous systems and the large amounts of cocatalysts needed to achieve the best catalytic activity.³ A breakthrough in this field was the use of heterogeneous catalytic systems. Although the activity of the supported systems is generally lower compared to the homogeneous systems,^{3,4} if *in situ* sup-

ported catalysts are employed, they can act as a reinforcement phase and control the polyolefin molecular architectures.^{5,6}

The most widely applied method to immobilize homogeneous olefin polymerization catalysts consists of anchoring metallocenes onto silica supports.⁷ Examples of silica-supported metallocene catalysts include systems prepared by direct deposition, MAO-pre-treated supports and covalent tethering. However, the direct anchoring of Cp₂ZrCl₂, for example, onto silica is a method where leaching occurs to a large extent. The second most leachable method is the MAO-pre-treatment prior to the anchoring of the metallocene.⁸ The leaching of materials prepared by direct anchoring or pre-treatment of the support with MAO can reach values between 37–80%.^{8–10}

A reasonable method to overpass this complicated issue is the covalent binding of organometallic compounds to the inorganic support,¹¹ which are known in the literature for their low percentage of leaching (about 3–7%) by MAO.¹² Plenty of strategies for anchoring of the organometallic complexes *via* covalent linkages between the support surface and one of the ligands of the complex have been described in the literature, including zirconocenes, ruthenium complexes and transition metal compounds.^{11,13–21}

^aMicro and Mesoporous Molecular Sieves Group, Institute of Chemistry, University of Campinas, Campinas, Sao Paulo, 13083-861, Brazil.

E-mail: gpmmm@iqm.unicamp.br

^bThe George and Josephine Butler Laboratory for Polymer Research, Department of Chemistry, University of Florida, Gainesville, Florida, 32611-7200, USA

†Electronic supplementary information (ESI) available. See DOI: 10.1039/c7dt03734a

‡Current address: Intel Corporation, 2501 NW 229th Ave, Hillsboro, OR 97214, USA.

With respect to the zirconium complexes, many issues regarding the tethering of a metallocene to the silica surface, which can limit the use of supported metallocenes in commercial olefin polymerization plants, have not yet been reasonably evaluated and explained: (i) What would be the role of the support in deactivation of the metallocenes during the immobilization reaction? (ii) What is the effect of metallocene interaction with the support? (iii) Does the morphology of the support affect the diffusion of the co-catalyst and monomers to the immobilized metallocenes? (iv) What are the consequences of this on the catalytic activity and properties of the polymers obtained?

Answers to these questions require a systematic and comprehensive study allowing a deep investigation of the metallocene, the support and the interaction between them. A comprehensive investigation of the influences of 2D and 3D inorganic structures on the catalytic performance, as well as on the properties of the metallocene complex, has not been reported previously from a structural point of view. This is because the tethering of organometallic compounds to a silica support is one of the most challenging routes to immobilize and characterize a catalyst system. There are two general routes that are employed: (i) building-up the ligand and subsequently the metal complex at the surface of the support or (ii) tethering a pre-synthesized catalyst. In the present work, our efforts focus on the understanding of both strategies in relation to the 2D and 3D inorganic structures as the support as well as the organic moieties in the catalytic system.

2. Experimental

2.1. Synthesis of the inorganic supports

The synthesis of MCM-41,²² Na-magadiite²³ and *n*-alkyl-ALPO-kanemite ($\text{AlPO}_3(\text{OH})_2[\text{CH}_3(\text{CH}_2)_{11}(\text{NH}_2)]_{0.43}[\text{CH}_3(\text{CH}_2)_3\text{NH}_2]_{0.57} = 43\text{dod},57\text{but-ALPO-kan}$)²⁴ was performed by following procedures previously developed by our group. For MCM-48 synthesis, the procedure reported by Castruita *et al.*²⁵ was followed. All the solids were pre-treated at 150–200 °C under vacuum ($\sim 10^{-5}$ mbar) for 12 h prior to the organic modifications.

2.2. Synthesis of the supported catalysts

All the air sensitive procedures were performed under a N_2 atmosphere using Schlenk lines and glovebox techniques.

2.2.1. Synthesis of 1. The catalyst was prepared by grafting of triethoxy(flouren-9-yl)silane on the surface of the inorganic support (Chart 1). The silane was prepared by the Grignard reaction. In parallel, the dry inorganic support, MCM-41, was suspended in toluene and stirred for 30 min under N_2 . In parallel, a solution of the silane in toluene was prepared and added to the support suspension and stirred under reflux for another 24 h. The final white solid was rinsed with toluene several times and dried under vacuum overnight at 60 °C. In the next step, diethyl ether (DEE) was condensed at -78 °C and *n*-butyllithium (1.6 M) was slowly syringed in it. The mixture was maintained under magnetic stirring for 12 h at

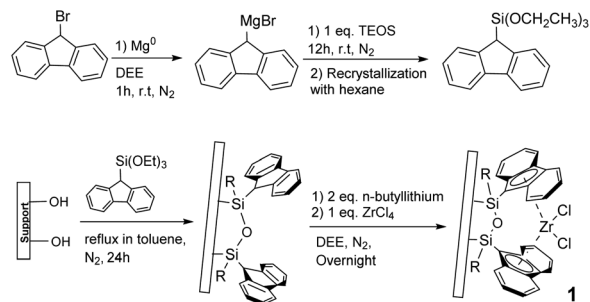


Chart 1 Synthesis of 1@MCM-41. R=OH, OEt, O–Si≡.

room temperature under N_2 . After, the solvent was removed by vacuum and zirconium tetrachloride was added, followed by the condensation of DEE at -78 °C. The reaction was performed under N_2 for another 12 h at room temperature. The solid was collected after filtration and rinsed with DEE. After drying under vacuum, a yellowish powder was obtained and collected inside of a glovebox and named 1@MCM-41.

2.2.2. Synthesis of 2 and 3. The synthesis of 12-bromo-octamethyl-octahydrodibenzofluorene ($\text{C}_{29}\text{H}_{37}\text{Br}$) was performed by first reacting 2,5-dimethyl-2,5-hexanediol with concentrated hydrochloric acid to isolate 2,5-dichloro-2,5-dimethylhexane. It was then added to 9-bromofluorene *via* a double cyclo Friedel-Crafts alkylation (Chart 2). The final solid was recrystallized with hexane.

Then, the initial step for preparing 2 and 3 over the supports was the grafting of aminopropyl groups on the surface of the supports. A suspension of the dry support in toluene (10 wt%) was stirred under N_2 for 30 min. Aminopropyltriethoxysilane ($\text{Si}(\text{OCH}_2\text{CH}_3)_3(\text{CH}_2)_3\text{NH}_2$) was dispersed in dried toluene and the solution was transferred to the support suspension. The reaction was stirred for 24 h under reflux at 65–70 °C. The solid was recovered by filtration and washed several times with toluene and dried under vacuum overnight at 60 °C. A solution containing 9-bromofluorene (from Aldrich) or 12-bromo-octamethyl-octahydrodibenzofluorene (Chart 2) in tetrahydrofuran (THF) was added to the NH_2 -modified support and the system was kept under stirring for 24 h. Then *N,N*-diisopropylethylamine (DIPEA) was added to remove the HBr byproduct. After, the solid was recovered by centrifugation and rinsed several times with THF and dried under vacuum overnight.

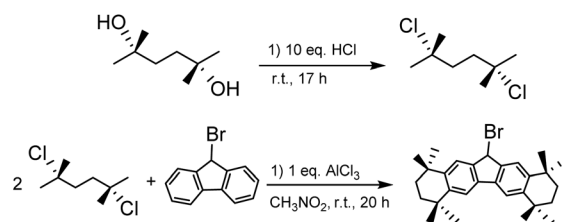


Chart 2 Synthesis of ($\text{C}_{29}\text{H}_{37}\text{Br}$).

The addition of Zr was performed using a Swivel Frit apparatus. The FI-NH₂-solids were previously treated at 70 °C under vacuum overnight to remove gases and solvent molecules possibly adsorbed. DEE was condensed at -78 °C and *n*-butyllithium (1.6 M) was slowly syringed in it. The mixture was maintained under magnetic stirring for 12 h at room temperature under N₂. After, the solvent was removed by vacuum and zirconium tetrachloride was added, followed by the condensation of DEE at -78 °C. The reaction was performed under N₂ for another 12 h at room temperature. The solid was collected after filtration and rinsed with DEE. After drying under vacuum, a yellowish powder was obtained and collected inside of a glovebox. The solids were named 2@magadiite, 2@MCM-48 and 3@MCM-41 (Chart 3).

2.2.3. Synthesis of 4. Catalyst 4 was synthesized by a multi-step procedure as described below (Chart 4). CTA-magadiite (magadiite swollen with cetyltrimethylammonium bromide)²⁶ was heated at 100 °C under vacuum prior to the organic modifications. Phenyltriethoxysilane was then grafted to the CTA-magadiite in the presence of refluxing toluene for 72 h under

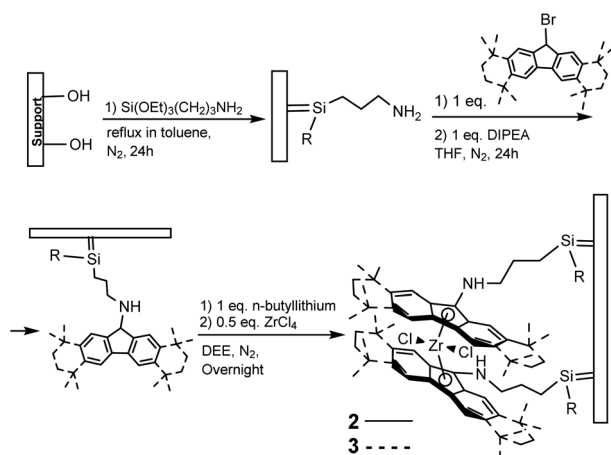


Chart 3 Synthesis of **2** (solid line) and **3** (dashed line) over the supports. R=OH, OEt, O-Si≡.

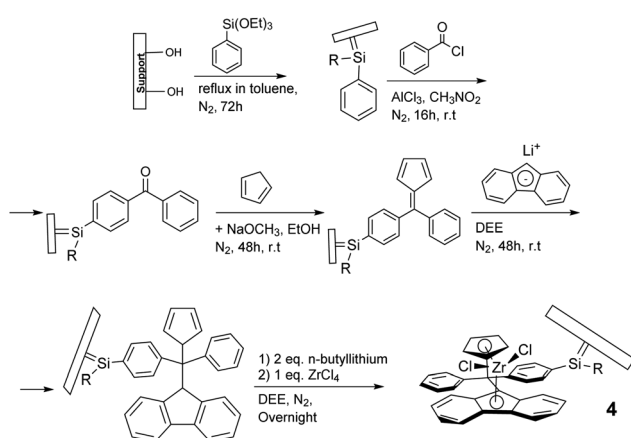


Chart 4 Synthesis of **4@magadiite**. R=OH, OEt, O-Si≡.

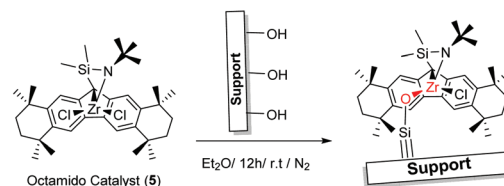


Chart 5 Anchoring of catalyst **5** to the inorganic supports.

nitrogen. The solid was rinsed and the Friedel-Crafts acylation reaction with benzoyl chloride in the presence of nitromethane for 16 h at room temperature was performed. The benzophenone-magadiite was rinsed with nitromethane and then reacted with cyclopentadienyl in the presence of sodium methoxide and ethanol under nitrogen for 48 h at r.t. The rinsed solid was reacted with fluorenyllithium for another 48 h at r.t. For the incorporation of Zr, the solid was treated with *n*-butyllithium in diethyl ether (DEE) for 12 h under N₂ at r.t. The solvent was removed by vacuum and ZrCl₄ was added to the system and DEE was condensed at -78 °C. The mixture was warmed up to r.t and stirred overnight under N₂. The solid was rinsed with DEE and dried under vacuum.

2.2.4. Synthesis of 5. The Oct-amido catalyst (**5**), Me₂Si(C₂₉H₃₆)(N-^tBu)ZrCl₂, was prepared as reported in the literature by Miller *et al.*²⁷ For the anchoring of **5** to the inorganic supports, the catalyst was placed in an air-free vessel with the support, DEE was added at -78 °C and this mixture was allowed to warm up to room temperature and stirred for 12 h (Chart 5). After rinsing the solid with DEE, the material was vacuum dried and the solid named **5@support** was stored in the glovebox.

2.3. Polymerization procedures

All the preparations were performed inside of a nitrogen-filled glovebox and the polymerization reactions were performed behind a blast shield. Methylaluminoxane (MAO) was purchased as a 30 wt% toluene solution and used as a dry powder obtained by vacuum removal of all volatiles. Toluene was dried over sodium, distilled and stored in a Straus flask.

A 85 mL glass Lab-Crest (Andrews Glass Co.) cylindrical polymerization vessel equipped with a stir bar was charged with a 1000 equiv. of solid MAO (*ca.* 0.193 g) and 25 mL of toluene. The reactor was then pressurized with ethylene, heated to 60–62 °C and allowed to equilibrate while stirring. After 10 min of equilibration, 1.0 mL of the catalyst suspension in toluene was injected (3.33 μmol of Zr per mL) into the vessel using a 2.5 mL Hamilton syringe. At the end, the reaction was vented and quenched by adding approximately 200 mL of 10 wt% aqueous HCl in MeOH to the polymer solution. The polymer was collected by filtration, rinsed with fresh methanol, and dried under high vacuum.

2.4. Characterization

X-ray diffraction (XRD) was performed in a XRD7000 Shimadzu apparatus with Cu radiation (Kα = 0.15406 nm). Slits of 5 mm

were used for dispersion and convergence radiation. High power decoupling (HPDEC) ^{29}Si NMR spectra of solid samples were recorded on a Bruker Avance III⁺ 300 MHz. The samples were spun at 10 kHz in a zirconia rotor. More than 1024 scans were obtained for proton-decoupled ^{29}Si NMR spectra, with 60 s delay time. For ^{13}C CP/MAS NMR spectra, >1000 scans were accumulated, using a 3 s delay between pulses, an acquisition time of 45 ms and a contact time of 4 s. The elemental analyses of carbon, hydrogen and nitrogen were performed using a CHNS/O Analyzer 2400 series II from PerkinElmer. The UV-Vis spectra of the solids were collected using a Varian Cary 5000 using a diffuse reflectance apparatus without dilution. The non-modified inorganic supports were used as a blank. For the liquid samples, a quartz cuvette was employed and diethyl ether was used as a solvent. To determine the Zr concentration in solution, the Lambert–Beer Law was employed. For that, a concentration *versus* absorbance curve was drawn to determine the molar absorptivity coefficient (ϵ). The Zr concentration in the solid was calculated by the difference between the amount of Zr added initially to the reaction and the amount remaining in the solution after the reaction. The content of zirconium was confirmed by X-ray fluorescence (XRF) as well as the amount of chlorine in the final catalysts. The XRF data were collected using a Shimadzu XRF-1800 equipment. The N_2 adsorption/desorption isotherms were obtained at cryogenic temperature using a NOVA 4200e equipment (Quantachrome Instruments). The samples were heated at 100 °C under vacuum for 24 h prior to the measurement. Surface areas were determined using the Brunauer–Emmett–Teller (BET) method and pore size distribution data were collected by the NLDFT method using cylindrical pores on silica for MCM-48 and BJH for MCM-41.

Polymers were characterized by thermal analyses in a TA Instruments Q5000 from room temperature up to 600 °C at a rate of 10 °C min^{-1} under nitrogen. Differential scanning calorimetry (DSC) was performed in a TA Instruments Q600 under helium at a rate of 10 °C min^{-1} from 0 °C to 200 °C. ^{13}C NMR samples were prepared by dissolving ~50 mg of polymer in 1.0 mL of 1,1,2,2-tetrachloroethane- d_2 . Spectra were obtained using a Varian INOVA 500, 125 MHz at 100 °C. A pulse of 70° was applied, the delay time was 5.5 s and 1500 scans were accumulated. The peak assignments and branching calculations were performed as described previously.^{28–30} The polymer molecular weights (M_w) were estimated by spin diffusion using the ^1H DOSY NMR technique in a Bruker Avance 500 MHz spectrometer as described by Grubbs *et al.*³¹

3. Results and discussion

The molecular structure of the supported catalysts is a key point for the understanding of the rules governing the stability and reactivity of the system during polymerization reactions. In this sense, detailed studies on inorganic materials as well as the organic part of the supported catalysts are the subject of great interest in this study. The molecular properties of these

systems were studied by a combination of physico-chemical methods, such as XRD diffraction, solid state UV-Vis and NMR spectroscopy.

3.1 The catalysts' structures

3.1.1 Catalyst 1@MCM-41. One of the attempts to tether a fluorene derivative catalyst on the surface of the inorganic support has been made by anchoring of the fluorene silane to the mesoporous solid MCM-41. The X-ray diffractogram of MCM-41 (Fig. 1, curve a) shows four main peaks below 7° 2θ , assigned to the (100), (110), (200) and (210) Miller's index related to hexagonal pore organization. After functionalization of the surface by fluorene silane, curve b, and the formation of catalyst 1@MCM-41 (curve c), there is a decrease in the intensity of these signals due to the presence of higher organic content in the solid.

In order to confirm the nature of porous MCM-41 before and after the organic modifications, N_2 adsorption/desorption isotherms were obtained and are seen in the ESI (SI_01†). Table 1 shows the physical parameters obtained from N_2 isotherms, such as the BET surface area, pore diameter and wall thickness.

The pores of 1@MCM-41 become slightly smaller as a result of immobilization of the zirconium complex. The increase in the wall thickness indicates the incorporation of the molecules inside the pores of MCM-41. The longest distance of the organic moiety is approximately 9.1 Å.³⁴ The pores of MCM-41 which possess an average diameter of 31 Å would provide more than enough space for the organic molecule to bind to the internal surface of MCM-41 cavities.

The ^{29}Si HPDEC/MAS NMR spectrum of MCM-41 (Fig. 2, curve a) shows a peak in the region of Q^4 [$\text{Si}(4\text{OSi})$] at -108 ppm and a peak of the Q^3 [$\text{Si}(3\text{OSi})(\text{OH})$] site is observed at -100 ppm. The immobilization of silane on the MCM-41 surface is confirmed by the presence of T-site signals in the

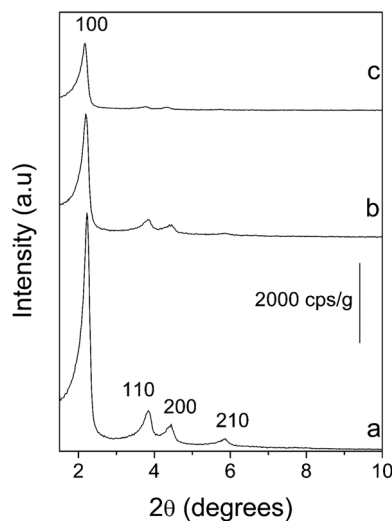


Fig. 1 XRD profile of (a) MCM-41, (b) fluorene grafted-MCM-41 and (c) assembled catalyst 1@MCM-41.

Table 1 Physical parameters of the tethered catalysts on MCM-41 and MCM-48 obtained by N₂ isotherms

Catalyst	<i>d</i> (nm)	Surface area BET (m ² g ⁻¹)	Total pore volume (cm ³ g ⁻¹)	Pore diameter <i>D</i> (nm)	Wall thickness ^a (nm)
MCM-41	<i>d</i> ₁₀₀ = 4.011	1033	0.863	3.143	1.488
1@MCM-41	<i>d</i> ₁₀₀ = 4.085	953	0.745	3.122	1.595
3@MCM-41	<i>d</i> ₁₀₀ = 4.283	498	0.447	3.110	1.886
MCM-48	<i>d</i> ₂₁₁ = 3.247	1047	0.835	3.775	0.699
2@MCM-48	<i>d</i> ₂₁₁ = 3.247	443	0.299	2.027	1.130

^a For MCM-41: Wall thickness = $\frac{2 \cdot d_{100}}{\sqrt{3}} - D$, where *D* = BJH average pore diameter.³² For MCM-48: Wall thickness = $\frac{a}{\xi_0} - \frac{D}{2}$, where *a* = $d_{hkl} \cdot \sqrt{h^2 + k^2 + l^2}$, $\xi_0 = 3.0919$ and *D* = NLDFT pore diameter.³³

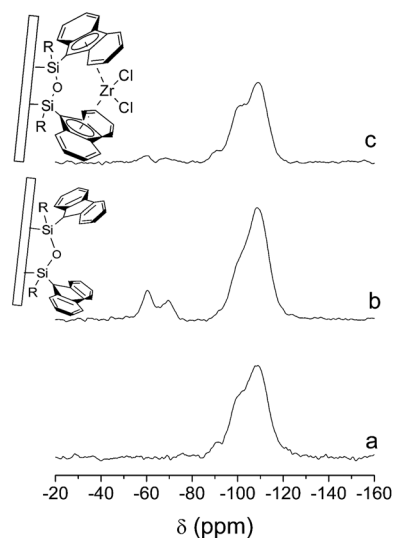


Fig. 2 ²⁹Si HPDEC MAS NMR spectra of (a) MCM-41, (b) fluorene grafted-MCM-41 and (c) assembled catalyst 1@MCM-41. R=OH, OEt, O-Si≡.

–50 and –75 ppm range in curve b, which accounts for 16% of Si sites. After the reaction with ZrCl₄, curve c, there is a decrease in the Si_T/Si_Q ratio from 16% (curve b) to 7% in 1@MCM-41 (curve c), indicating partial leaching of silane in the presence of *n*-butyllithium (used to generate the fluorenyl anion in the formation of 1@MCM-41). The organic content in the final catalyst 1@MCM-41 is confirmed by the ¹³C CP/MAS NMR spectrum as shown in Fig. 3A. The presence of the aromatic carbons in the region of 100–150 ppm as well as the Si–C bond at 30 ppm can be observed, proving that the organic part of the catalyst is still attached to the surface of MCM-41.

The UV-Vis spectra of the fluorene-modified MCM-41 before and after the reaction with ZrCl₄ are shown in Fig. 3B. A band with a maximum of 288 nm is observed, assigned to the electronic transitions of the fluorene ring (curve a). This same band, when in the presence of zirconium (curve b), is displaced in the region between 300 and 450 nm (with a maximum at 320 nm) and it is broadened due to the fluorene-Zr LMCT transitions, indicative of the formation of 1@MCM-41 as desired. In this same spectrum, curve b, a well-defined band at 224 nm is observed, typical of the O²⁻ → Zr⁴⁺ charge transfer from Zr in a tetrahedral conformation.^{35,36}

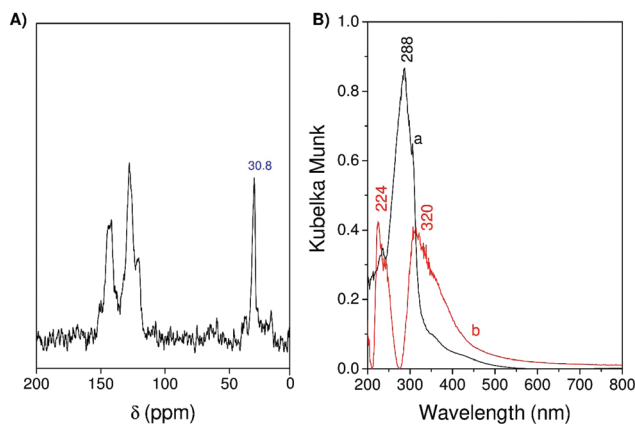
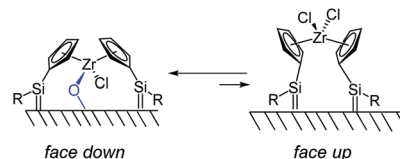


Fig. 3 (A) ¹³C CP/MAS NMR spectrum of 1@MCM-41 catalyst. (B) Solid state UV-Vis spectra of (a) fluorene grafted-MCM-41 and (b) assembled catalyst 1@MCM-41.

This band is observed if the catalyst (or part of it) exhibits a face-down type configuration³⁷ with the surface as shown in Scheme 1.

Table 2 reports the loading of the grafted fluorenyl and zirconium contents on the supported systems. In the case of 1@MCM-41, the fluorenyl/Zr molar ratio of 2.9/1.0 indicates that for every two fluorenyl group, there is one zirconium center, forming the complex, and about 30% of the fluorenyl groups are not a zirconium complex, remaining as a free ligand on the surface of the support. The Zr/Cl molar ratio of 1.0/1.1 is in agreement with the proposed face down Zr complex with the support surface, indicated by the UV-Vis spectra and shown in Scheme 1. The face down and face up effects would greatly impact the catalyst activity since the monomer and cocatalyst access to the metal center can be sig-



Scheme 1 Face-down and face-up conformation of catalyst 1@MCM-41. Only the cyclopentadienyl metal centre is shown for clarity. R=OH, OEt, O-Si≡.

Table 2 Elemental analysis of the tethered catalysts

Catalyst	Fluorenyl content ^a (mmol g ⁻¹ solid)	N content ^a (mmol g ⁻¹ solid)	Zr content ^b (mmol g ⁻¹ solid)	Cl content ^b (mmol g ⁻¹ solid)	Cl : Zr : N
1@MCM-41	0.455	—	0.157	0.171	1.1 : 1.0 : 0
2@Magadiite	3.048	3.254	1.023	2.647	3.2 : 1.0 : 2.6
2@MCM-48	3.641	3.852	1.618	1.855	1.2 : 1.0 : 2.4
3@MCM-41	1.395	1.433	0.420	0.699	1.6 : 1.0 : 3.4

^a Elemental analysis (CHNO). ^b XRF analysis.

nificantly affected by these face-down and face-up conformations.

3.1.2 Catalysts 2@magadiite, 2@MCM-48 and 3@MCM-41. Due to the simplicity of syntheses of amino-modified supports, they have been studied for many different applications. One of their uses is for organometallic olefin polymerization catalysts. In this application, tethering can prevent catalyst leaching in slurry phase processes, for example. Here, primary-amine-functionalized materials of varying 2D and 3D morphologies have been prepared and used as supports for tethered catalysts. In this method, the metal centre would be distant from the surface by a three-carbon alkyl linker.

3.1.2.1 Catalyst 2@magadiite. Fig. 4 shows the X-ray diffractogram of magadiite during the preparation of **2** on its surface. Curve a presents the diffractogram of CTA-magadiite whose basal spacing is 3.17 nm (2.78° 2θ).

The presence of a long chain organic cation like CTA⁺ (C₁₆H₃₃(CH₃)₃N⁺) is important in the process of organo-functionalization because it allows the expansion of the interlamellar space and makes it more organophilic, facilitating the access of the organic molecules to the space between the lamella of the silicate. After the aminopropyl grafting step, the

X-ray diffraction (curve b) of the solid shows that the peaks in the region of 22–30° 2θ, which already indicated the turbostratic effect due to the presence of CTA⁺, suggest a significant decrease in the organization of the lamella, one in relation to another. This effect is pronounced after the reaction with fluorene and the incorporation of Zr into the complex built on the magadiite's surface, curves c and d, respectively. After the reaction with fluorene (curve c), there is a decrease in the interlayer space to 2.67 nm (3.30° 2θ), probably caused by the π–π interactions of the aromatic structure of fluorene as well with the magadiite surface. When the catalyst 2@magadiite is finally assembled, curve d, the interlamellar plane displacement is observed at smaller angles (2.28° 2θ/3.87 nm), indicating an increase of 0.7 nm of the interlamellar space compared to the starting CTA-magadiite, reflecting the accommodation of the organic on catalyst 2@magadiite.

Fig. 5a presents the typical magadiite ²⁹Si resonances assigned to Q³ [Si(3OSi)(OH)] at –99 ppm and two peaks in the Q⁴ [Si(4OSi)] region at –112 and –109 ppm. The functionalization of the CTA-magadiite surface can be seen in curve b of Fig. 5. One can observe the appearance of T² (RSi(OSi)₂OH) and T³ (RSi(OSi)₃) signals at –59 and –67 ppm, respectively, corresponding to 19% of the sites (Si_T/Si_Q ratio),

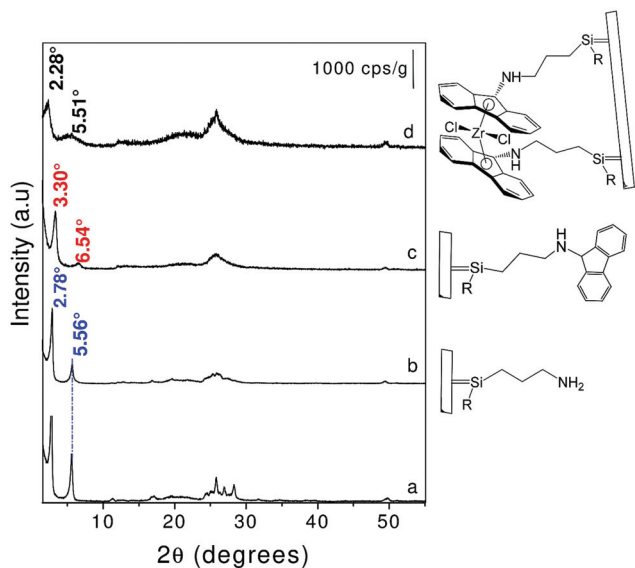


Fig. 4 XRD diffractograms of (a) CTA-magadiite, (b) NH₂-modified magadiite, (c) fluorene-NH₂-magadiite and (d) **2**@magadiite. R=OH, OEt, O–Si≡.

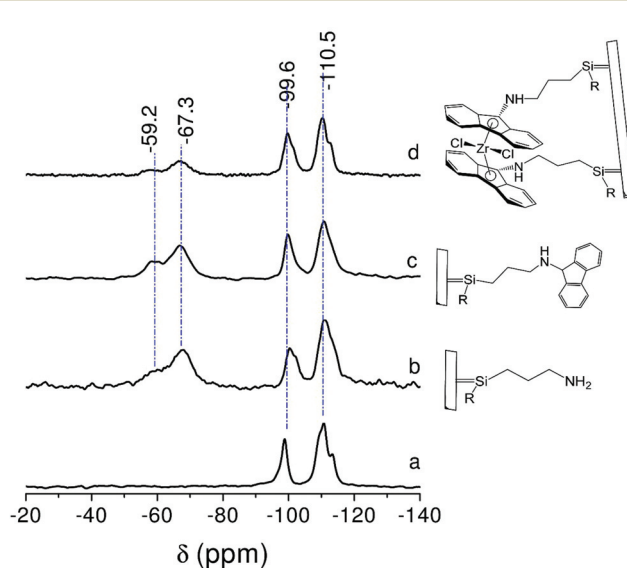


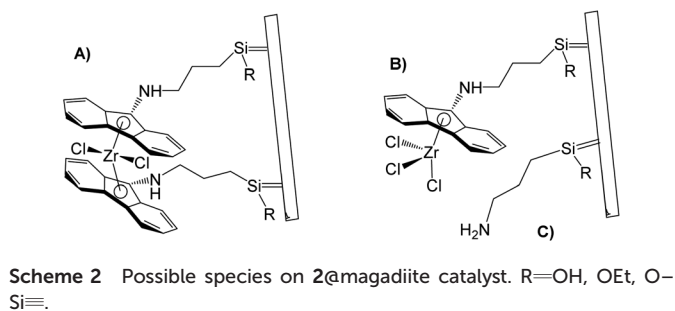
Fig. 5 ²⁹Si HPDEC/MAS NMR spectra of (a) CTA-magadiite, (b) NH₂-modified magadiite, (c) fluorene-NH₂-magadiite and (d) catalyst **2**@magadiite. R=OH, OEt, O–Si≡.

which is kept after addition of fluorene (curve c). The final catalyst 2@magadiite exhibits a lower amount of T sites (curve d) compared to the functionalized precursor (curve b). The Si_T/Si_Q ratio decreases to 11%, indicating that there was partial loss of the surface aminopropyl groups in the presence of *n*-butyllithium employed for the addition of zirconium.

The organic moieties of catalyst 2@magadiite were also evaluated by ^{13}C CP/MAS NMR (Fig. 6). The ^{13}C NMR spectrum of CTA-magadiite (curve a) shows the characteristic peaks of the all-*trans* configuration of the organic CTA⁺ cation, which keeps the magadiite's lamella separated. The aminopropyl group can be observed in the spectrum of curve b along with CTA⁺. After the reaction of the aminopropyl groups with fluorene, curve c, the appearance of a peak at 61.4 ppm was observed (dotted square in curves c and d of Fig. 6) assigned to the bond formed between the -NH₂ group and the fluorene, leading to the immobilized fluorene on the solid. In addition, the aromatic carbons from fluorene moieties appear in the region of 90 to 160 ppm as expected. After the reaction with ZrCl₄, curve d, the catalyst remains bonded to the solid as indicated by the presence of the N-fluorene bond (peak in 61 ppm) and the fluorene aromatic carbons between 90 and 160 ppm.

The elemental analysis of 2@magadiite in Table 2 shows the Cl/Zr/N molar ratio of 3.2/1.0/2.6. This result indicates that, beyond the proposed system which should be ideally Cl/Zr/N molar ratio of 2/1/2 (species A in Scheme 2), there are some possible species that cannot be neglected like the trichloride zirconium complexes on the surface (species B in Scheme 2) as well as a few free aminopropyl groups in the solid (species C in Scheme 2).

3.1.2.2 Catalyst 2@MCM-48. Solids in which pore sizes have fixed diameters, like MCM-41 and MCM-48, were also investigated in the preparation of tethered catalysts for olefin



Scheme 2 Possible species on 2@magadiite catalyst. R=OH, OEt, O-Si.

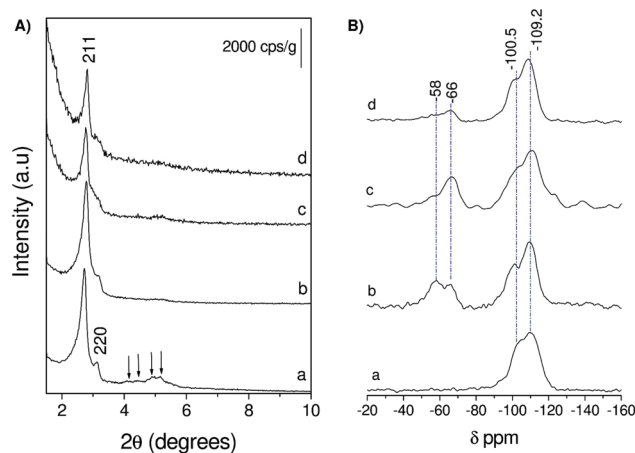


Fig. 7 (A) XRD profile and (B) ^{29}Si HPDEC NMR of (a) MCM-48, (b) NH₂-modified MCM-48, (c) fluorene-NH₂-MCM-48 and (d) catalyst 2@MCM-48.

polymerization. MCM-48 is formed in a symmetric space group of the *Ia3d* type with cubic organization of pores. The typical MCM-48 diffractogram (Fig. 7A, curve a) contains the

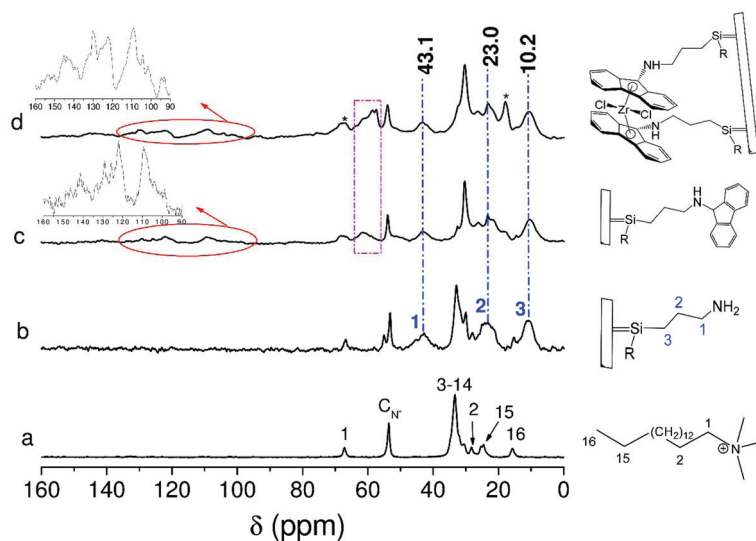


Fig. 6 ^{13}C CP/MAS NMR spectra of (a) CTA-magadiite, (b) NH₂-modified magadiite, (c) fluorene-NH₂-magadiite and (d) catalyst 2@magadiite. * CH₂ and CH₃ from DEE solvent (66 and 16 ppm).

peaks assigned to the planes (211), (220), (321), (400), (420) and (332).

Here, the same procedure as that of aminopropyl-grafting, followed by the fluorene reaction with the -NH_2 groups and zirconium addition, reported above for magadiite, was performed. One can observe that after the organic modifications, curves b–d in Fig. 7, the main diffraction peaks (211) and (220) are broadened. This is probably due to the increase in the organic content (that does not diffract) as well as the heterogeneous distribution of the organic groups in the MCM-48 channels.

The pore volume and diameter of 2@MCM-48 are significantly smaller than the non-modified MCM-48 (see Table 1) as well as the surface area. The approximate 50% decrease in the surface area can be assigned to the successful anchoring of the catalyst on the internal surfaces of the mesoporous material. This is confirmed by the decrease in the adsorption pore volume from 0.8 to 0.3 $\text{cm}^3 \text{g}^{-1}$ and the wall thickening from 0.7 nm to 1.1 nm with the addition of the organic component similar to 1@MCM-41.

Surface functionalization of these materials is confirmed by ^{29}Si NMR spectra (Fig. 7B), where T sites are observed between -40 and -70 ppm (curve b). After insertion of fluorene followed by the reaction with ZrCl_4 , there is a decrease in the $\text{Si}_\text{T}/\text{Si}_\text{Q}$ ratio from 28% (curve b) to 8% in the final catalyst 2@MCM-48 (curve d), the effect of the partial hydrolysis of some aminopropyl groups as mentioned before for the other systems. Regarding the organic content on 2@MCM-48, Fig. 8 (curve a) displays the ^{13}C CP/MAS NMR spectrum of the aminopropyl functionalized MCM-48 with characteristic peaks of the immobilized aminopropyltriethoxysilane moiety. After the reaction with fluorene, curve b, the solid presents peaks in the region of 100 to 160 ppm due to the ^{13}C atoms of the fluorene aromatic system and a broad and intense peak at 61 ppm

assigned to the bonding of the -NH group to fluorene, again confirming the immobilization of fluorene to the mesoporous silica surface. After assembling of catalyst 2@MCM-48, curve c, the ^{13}C NMR profile is maintained.

The Cl/Zr/N molar ratio of 2@MCM-48 is 1.2/1.0/2.4. This system is slightly different from 2@magadiite: although both catalysts can exhibit free aminopropyl groups like species C in Scheme 2, while 2@magadiite presents trichloride zirconium complexes and 2@MCM-48 presents monochloride zirconium species.

3.1.2.3 Catalyst 3@MCM-41. Sterically expanded fluorene was also synthesized over the surface of MCM-41 in order to investigate its performance on olefin polymerization. Catalyst 3@MCM-41 was synthesized as reported for 2@magadiite and 2@MCM-48, using an Oct-fluorene derivative instead of fluorene. The powder XRD diffractograms of the solids after each reaction step are reported in the ESI (Fig. SI_02†). MCM-41 presented sharp, well-defined peaks which, in the final assembled 3@MCM-41 catalyst, are broadened as a result of a slightly disturbed scattering contrast.³⁸ As the effect might be inhomogeneous or affect pores differently, some will show thicker walls than others, changing a_0 and creating a set of peaks, slightly spaced one from the other compared to the non-organic modified support. The net result is broadening of the signals.

The grafting of the surface by the silane is confirmed by ^{29}Si HPDEC/MAS NMR, Fig. 9. After aminopropyl grafting, curve b, the evident appearance of signals referring to the T³ sites ($\text{RSi}(\text{OSi})_3$) at -67 ppm is observed, confirming the incorporation of the aminopropyl pendent to the inorganic struc-

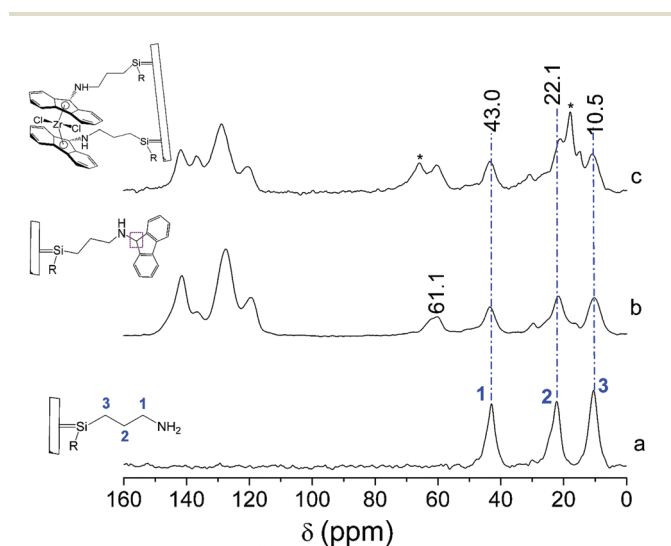


Fig. 8 ^{13}C CP/MAS NMR of (a) NH_2 -modified MCM-48, (b) fluorene- NH_2 -MCM-48 and (c) catalyst 2@MCM-48. $\text{R}=\text{OH}$, OEt , $\text{O-Si}\equiv$. * CH_2 and CH_3 from DEE solvent (66 and 16 ppm).

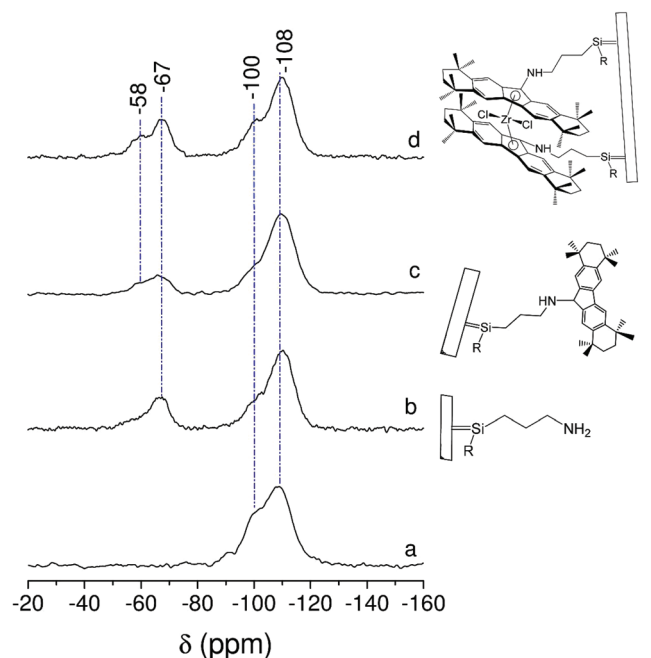


Fig. 9 ^{29}Si HPDEC NMR spectra of (a) MCM-41, (b) NH_2 -modified MCM-41, (c) Oct-fluorene- NH_2 -MCM-41 and (d) catalyst 3@MCM-41. $\text{R}=\text{OH}$, OEt , $\text{O-Si}\equiv$.

ture. When reacting with Oct-fluorene (curve c) and ZrCl_4 (curve d) there is the appearance of T^2 sites ($\text{RSi}(\text{OSi})_2\text{OH}$) at -58 ppm, resulting from the partial loss of some aminopropyl groups. The organic moieties were investigated by ^{13}C CP/MAS NMR spectroscopy and present a similar behaviour described for 2@magadiite or 2@MCM-48 catalysts and can be seen in the ESI (SI_03†). The catalyst is attached to the MCM-41 surface as indicated by the peak at 60 ppm in the ^{13}C NMR spectrum.

The Oct-fluorenyl content was determined as 1.395 mmol g^{-1} of solid (Table 2). Also, catalyst 3@MCM-41 presents a Cl/Zr/N molar ratio of $1.6/1.0/3.4$, which means that, as observed for 2@MCM-48, free aminopropyl groups and monochloride zirconium species as well can be present in the solid. All of the possible species tethered on the surface of MCM-41 might be at the internal cavities of the support. The significant decrease in the surface area from 1033 m^2 g^{-1} to 498 m^2 g^{-1} can be assigned to the anchoring of the catalyst on the surface of the MCM-41. The wall thickening from *ca.* 1.5 nm to *ca.* 1.9 nm indicates that the catalyst was assembled in the inner part of the support. Moreover, there is a plenty of room for the catalyst to be built inside of the pore: the maximum length that catalyst 3 can have is *ca.* 13.5 Å (ref. 34) while MCM-41 possesses 31.4 Å of pore diameter.

Catalysts 2@magadiite, 2@MCM-48 and 3@MCM-41 were prepared using the aminopropyl group as a bridge for their immobilization onto the surface of the supports. The ^{13}C peaks of the aminopropyl group exhibited narrow resonances reflecting the high flexibility or freedom of the molecular moiety. After insertion of fluorene or Oct-fluorene, these propyl chain peaks are broader especially when MCM-41 and MCM-48 are the supports, indicating that the degree of flexibility of the aminopropyl chain decreased. This effect is less evident in magadiite due to its expandable interlayer space and the presence of interlamellar CTA^+ . Also, in all cases the peak at 60 ppm, assigned to the $-\text{NH}$ -Fluorene bond is quite broad, indicating the participation of different conformations and possible interactions of the organic part with the surface of the support. These surface interactions directly affect the catalytic activity of the metal centre during the polymerization of olefins and can be understood by UV-Vis spectroscopy.

3.1.2.4 Catalysts 2@magadiite, 2@MCM-48 and 3@MCM-41 from the point of view of UV-Vis spectroscopy. Looking at the UV-Vis spectra of the catalysts shown in Fig. 10, a band can be observed between 270 and 320 nm, present in all solids, characteristic of the π interactions of the fluorene aromatic ring with the pair of electrons of the NH group to which it is attached,³⁹ besides a band in the region of 431 nm due to the interaction of the fluorenyl anion with the zirconium, assigned to ligand–metal charge transfer (LMCT) fluorene \rightarrow Zr^{4+} .

In 2@MCM-48 and 3@MCM-41 an intense band in the region of 220 nm is observed and it seems possibly due to the charge transfer $\text{O}^{2-} \rightarrow \text{Zr}^{4+}$ in a tetrahedral configuration. For this charge transfer to occur, the metal atom of the catalyst should interact with the surface of the carrier as shown in Scheme 3, and the Cl/Zr molar ratio is expected to be lower

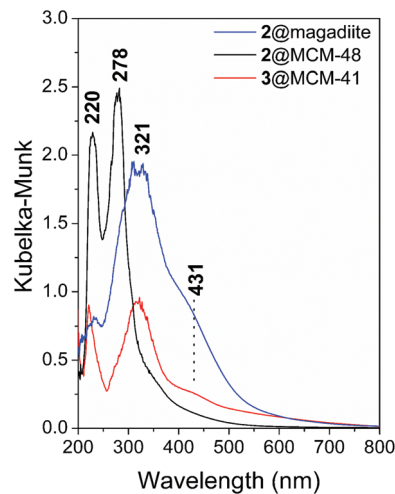
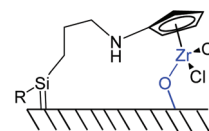


Fig. 10 UV-Vis spectra of the solid catalysts 2@magadiite, 2@MCM-48 and 3@MCM-41.



Scheme 3 Schematic representation of the interaction of the organic part of the catalyst with the surface of the support. Only the cyclopentadienyl metal centre is shown for clarity. R=OH, OEt, O-Si≡.

than 2/1 as seen for the set of catalysts shown here. This interaction with the surface occurs more intensely in mesoporous solids, whose pore arrangements are rigid and confine the catalyst within a more restricted space. In these cases, the Zr center interacts with the supports' surface at the expense of the organic chain flexibility. When the catalyst is built on the surface of magadiite, which has expandable interlayer space, this effect was not observed. This confinement has an important effect on the production of polyolefins and is discussed next.

3.2 The polymerization of olefins by tethered catalysts

Catalysts 1@MCM-41, 2@magadiite, 2@MCM-48 and 3@MCM-41 were employed for the polymerization of ethylene as well as propylene and are summarized in Table 3. Catalyst 1@MCM-41 did not work under any of the conditions employed for both ethylene and propylene polymerizations. As seen by UV-Vis spectra shown in Fig. 3B, the metal centre becomes irreversibly blocked in a face-down configuration, in addition to limiting the conformational freedom of the catalyst on the surface, preventing the capture of the monomer to polymerize. If the catalyst is built too close to the inorganic surface of the support, the interaction of the metal center with the surface can lead to some drawbacks, including the possible formation of deactivated catalysts through their interactions with the support material. As illustrated in Scheme 1,

Table 3 Polymerization results using tethered catalysts 1@MCM-41, 2@magadiite, 2@MCM-48 and 3@MCM-41

Entry	Catalysts	Monomer	Activity (kg per mol Zr per h)	T_M (°C)	T_C (°C)	T_{max} of decomposition (°C)
1	1@MCM-41	Propylene	0	—	—	—
2	1@MCM-41	Ethylene	0	—	—	—
3	2@Magadiite	Propylene	14	—	—	—
4	2@Magadiite	Ethylene	656	135	120	394
5	2@Magadiite	Ethylene ^a	595	125	118	452
6	2@MCM-48	Propylene	0	—	—	—
7	2@MCM-48	Ethylene	353	130	117	398
8	2@MCM-48	Ethylene ^a	301	131	113	451
9	3@MCM-41	Propylene	0	—	—	—
10	3@MCM-41	Ethylene	30	133	118	396

Zr = 3.33 μ mol. PE: 5.5 bar, 60 °C, 10 min. PP: 30 mL of propylene, r.t., 30 min. MAO/Zr = 1000. ^a 2.5 mmol of 1-octene was added to the reactor.

1@MCM-41 depicts a metallocene molecule bonded to the support by two short tether points. One would expect not only to confine movement (translational and rotational) of the molecule, but also to make the metal center in the face-up configuration, *i.e.*, facing away from the silica surface. The face-up configuration ensures sufficient accessibility of the metal center by monomers during polymerization. However, what was found in the present work, following the strategy proposed, is that the movement restriction by two tether points to the surface is not strong enough, so the bonded molecule may still take a face-down configuration. When an alkyl chain is added between the support and the catalyst metal centre as in catalysts 2@magadiite, 2@MCM-48 and 3@MCM-41, the scenario changes a little. These three catalysts showed low activity in the polymerization of ethylene and were completely inactive in the preparation of polypropylene. Other conditions were tested and there was no formation of polypropylene.

The interesting results come from the ethylene polymerization reaction (Table 3, entries 4, 7 and 10): a single peak in DSC curves between 130–135 °C was observed in all samples, suggesting the formation of HDPE (High Density PolyEthylene). Ethylene polymerization produced linear PE, as observed by the single peak at 30 ppm in the ¹³C NMR spectrum (ESI SI_04†), showing the role of the carrier as a limiting factor in the insertion of branching even as small as a methyl group as in the case of propylene. Moreover, in order to induce branching formation on the PE chain, 1-octene was added to the polyethylene synthesis using 2@magadiite and 2@MCM-48 as catalysts (entries 5 and 8 of Table 3, respectively). However, there was no increase in the degree of branching of PE as observed by the presence of a single peak at 30 ppm in the ¹³C NMR spectrum (ESI SI_04†).

Using the aminopropyl chain, the covalent tethering method was expected to avoid the disadvantage of the direct grafting of the fluorene method by putting a covalent spacer between an active site and the support surface. In fact, it helped the system and some polyethylene was synthesized. But the flexibility of a long chain also provides the active site a pseudo-solution environment, *i.e.*, there is still some degree of flexibility of the chain that provides a route for the direct interaction of the active site with the surface, so some of the active

sites are in a similar situation as before and the polymerization catalyst cannot reach its best performance.

3.3 Catalyst 4@magadiite

Keeping these results in mind, another strategy for the immobilization of olefin polymerization catalysts was performed using a multi-step methodology in order to construct an assembled catalyst, similar to the homogeneous one, on the surface of magadiite. So, first CTA-magadiite (Fig. 11, curve a) was functionalized with triethoxyphenylsilane (phenyl-CTA-magadiite), curve b. Then, through a Friedel Crafts acylation, the benzophenone molecule was bonded to the support (benzophenone-CTA-magadiite), curve c. After condensation of the aromatic cyclopentadienyl to the system, the diphenylfulvene group was anchored to the support (diphenylfulvene-CTA-magadiite), curve d. Next, the reaction with fluorene led to the formation of a $\text{Ph}_2\text{C}(\text{C}_5\text{H}_5)(\text{C}_{13}\text{H}_9)$ ligand bound to magadiite, curve e. The final magadiite catalyst is obtained after the reaction of ZrCl_4 with the solid, curve f, leading to the catalyst 4@magadiite. It is observed that during diphenylfulvene-CTA-magadiite formation (curve d) the characteristic interlamellar distance increases from 3.17 nm to 3.82 nm, accommodating

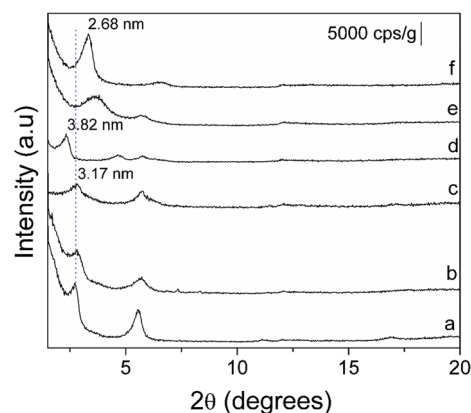


Fig. 11 XRD diffractograms of (a) CTA-magadiite, (b) phenyl-CTA-magadiite, (c) benzophenone-CTA-magadiite, (d) diphenylfulvene-CTA-magadiite, (e) $\text{Ph}_2\text{C}(\text{C}_5\text{H}_5)(\text{C}_{13}\text{H}_9)$ -magadiite and (f) catalyst 4@magadiite.

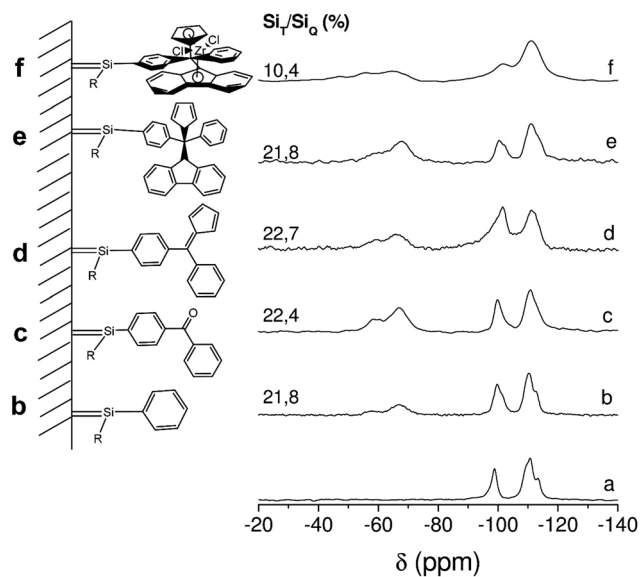


Fig. 12 ^{29}Si HPDEC/MAS NMR spectra of (a) CTA-magadiite, (b) phenyl-CTA-magadiite, (c) benzophenone-CTA-magadiite, (d) diphenylfulvene-CTA-magadiite, (e) $\text{Ph}_2\text{C}(\text{C}_5\text{H}_5)(\text{C}_{13}\text{H}_9)$ -magadiite and (f) catalyst 4@magadiite. R=OH, OEt, O-Si \equiv .

the ligand. By adding fluorene and Zr, curves e–f, the interactions between the aromatic rings force the system to approach the lamella and the interlayer space reduces to 2.68 nm.

The ^{29}Si NMR spectra (Fig. 12) show that there was a decrease in the concentration of T sites from 22 to 10% when catalyst 4@magadiite is assembled after addition of ZrCl_4 , curve f, resulting in the partial loss of the silane in the presence of *n*-butyllithium employed for the addition of zirconium. In fact, if we consider that the molar absorptivity is not changed from the free ligand to the coordinated situation, the UV-Vis spectrum (Fig. 13) shows that after the reaction with Zr, there is a significant decrease of the aromatic organic absorption in the region of UV-Vis, indicating that there was, in fact, leaching of organic part from the support catalyst. When tested for the polymerization of ethylene and propylene, the catalyst 4@magadiite had no activity in the reactions. Several reaction conditions were tested, but no polymer was obtained. The final solution, after addition of acidified methanol, was rotoevaporated in an attempt to precipitate some polymeric materials, but without success, proving that the metallocene complex is sensitive to the reaction conditions employed for its systems and was removed from the structure when the multi-step methodology was chosen to tether the metallocene to the support surface.

3.4. Catalyst 5@layered supports

The results shown here point to the intrinsic influence of the support on the polymerization processes catalysed by the metallocene center: because the presence of the support in the surroundings of the metallocene plays the role of a bulky

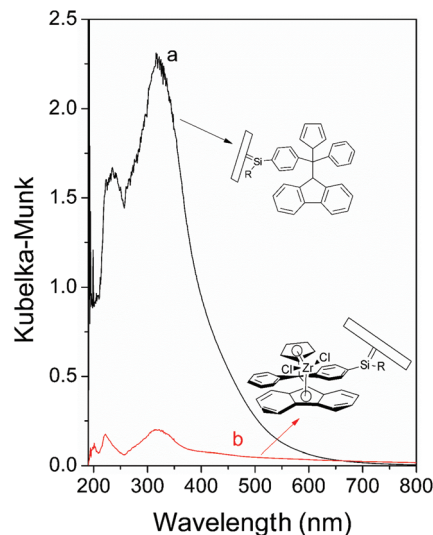


Fig. 13 UV-Vis spectra of (a) $\text{Ph}_2\text{C}(\text{C}_5\text{H}_5)(\text{C}_{13}\text{H}_9)$ -magadiite and (b) catalyst 4@magadiite (before and after ZrCl_4 addition, respectively). R=OH, OEt, O-Si \equiv .

ligand, it reflects in steric and electronic effects of smaller or higher order; at the end, it influences the reaction mechanism and the production of the polymer. The catalysts built farther away from the surface had low activity in the production of PE due to the formation of a more stable species coming from the interaction with the surface. Catalysts built close to the surface had no activity in the production of olefins. Two factors are related: (i) the system can be locked on a face-down configuration with the surface or (ii) the system is sensitive to the reactive conditions and ends up being leached from the structure.

The Zr–O interactions are difficult to eliminate in these systems and seem to be certain using the current strategies. A good supporting technique should not only strongly immobilize a metallocene catalyst, *i.e.*, no leaching of active species from the support, but it also preserves the most useful features of the catalyst.

Thus, in order to prepare an efficient heterogeneous metallocene catalyst, the direct deposition approach was taken into consideration. This method can be very convenient for metallocene immobilization. In a typical process, the pre-treated support is stirred with a solution of a metallocene compound under an inert atmosphere at room temperature or elevated temperatures for a period of time. Then, the slurry is filtered, and the remaining solid product is washed with solvent several times to remove weakly adsorbed metallocene molecules. The washed product is dried under vacuum to remove the solvent. The metallocene compound reacts with hydroxyl groups on the silica surface and bond to the surface through a M–O–Si bond (Chart 5). Good catalyst performance can be reached with this strategy.^{40,41}

In this sense, the Oct-amido catalyst (catalyst 5) was reacted with different layered supports and the final solids represent a survey of the types of supports that could be used with the Oct-amido catalyst. Fig. 14A and B display the XRD diffractograms

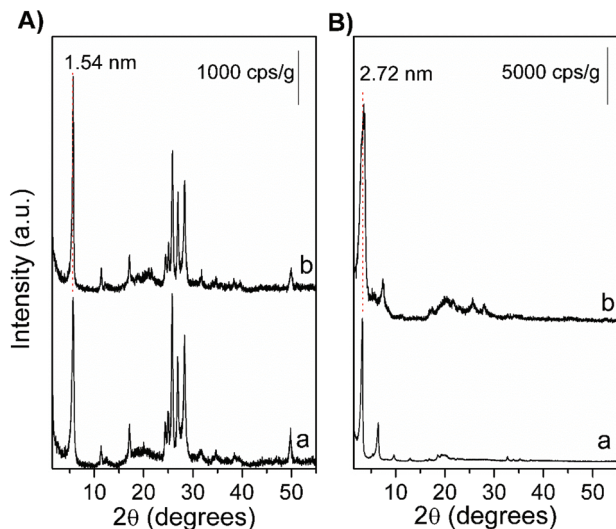


Fig. 14 XRD diffractograms of (A) magadiite (a) and 5@magadiite (b) and (B) *n*-alkyl-AlPO-kan (a) and 5@*n*-alkyl-AlPO-kan (b).

of the layered supports magadiite and *n*-alkyl-AlPO-kan, respectively, before and after anchoring of the Oct-amido cata-

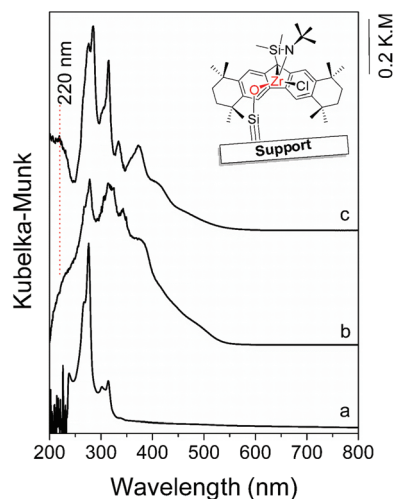


Fig. 15 UV-Vis spectra of homogeneous Oct-amido catalyst 5 in CHCl₃ (a), 5@magadiite (b) and 5@*n*-alkyl-AlPO-kan (c).

lyst. No exfoliation can be observed regarding the stacking of the lamella peak below 5° 2θ. Solid state UV-Vis spectra was used to certify that the catalyst was attached to the support surface (Fig. 15). The presence of a peak at 220 nm shows that the Zr–O bond was formed and indicates that the catalyst is attached to the surface. The increase in absorbance around 345–415 nm also indicates the presence of the support in the sample.

Once 5 was adsorbed onto the supports, polymerizations of ethylene were performed. The layered supports were chosen because of their special ability to accommodate guest compounds in between the layers and they can also exfoliate to better accommodate bulky molecules or polymers. The results for polymers made from homogeneous 5, 5@*n*-alkyl-AlPO-kan and 5@magadiite are shown in Table 4.

The homogeneous catalyst polymerizations, under the conditions employed, have an activity of about 2000 kg of PE per mol Zr per h with a melting temperature of 112 °C. Branching is one of the most important features of catalyst 5: it is able to produce highly branched PE and low *M_w* (about 1000 g mol⁻¹) from a source of pure ethylene, without the addition of comonomers. Overall, the supported catalysts had lower activities compared to the homogeneous catalyst possibly due to the steric hindrance of the layers, making it difficult to prepare large amounts of the polymer or for monomer to diffuse into the layers as well as some bimolecular deactivation from the interaction of the catalyst and support.

The melting temperatures for all of the supported systems increased to 134–135 °C. This is due to an absence of any branching. This result was quite surprising. By supporting this catalyst on inorganic supports, either the active site becomes sterically hindered and will no longer accept the large α-olefins made *in situ* to produce branching or it affects the mechanism by which the catalyst affects the β-hydride elimination reaction. What is more interesting is that this catalyst, once activated by MAO, is possibly detached from the support but is contained within the layers and this still drastically changes the mechanism and forces the catalyst to only produce linear PE (see the ¹³C NMR spectrum in ESI SI_05†).

To help elucidate whether the support is affecting the β-hydride elimination portion of the mechanism or whether it is hindering the active site and preventing the α-olefins from inserting into the polymer backbone, copolymerization with

Table 4 Ethylene polymerizations with supported 5

Catalyst	Zr loading on the support ^a (mmol Zr per g of solid)	Activity (kg of PE per mol Zr per h)	<i>T_M</i> (°C)	<i>M_w</i> ^b (g mol ⁻¹)	Branching ^c		
					<i>N_E</i>	<i>N_L</i>	<i>N_T</i>
5 Homogeneous	—	2120	112	1048	6.3	39.5	45.8
5@Magadiite	0.0455	599	135	20 036	0	0	0
5@ <i>n</i> -alkyl-AlPO-kan	0.0555	750	134	—	0	0	0

Polymerizations were performed at 5.5 bar of ethylene, 60 °C for 10 min, with 3.3 μmol of Zr and 1000 equivalents of MAO. ^a Calculated by the difference between the amount of catalyst added and the amount of catalyst remained in solution after reaction, using UV-Vis spectroscopy. ^b Estimated by ¹H DOSY NMR. ^c Number of ethyl (*N_E*), long (*n*-hexyl or greater, *N_L*) and total branches (*N_T*) per 1000 carbons.

Table 5 Ethylene/1-octene copolymerizations with 5@magadiite

1-Octene (mmol)	Activity (kg of PE per mol Zr per h)	T_M (°C)	Branching		
			N_E	N_L	N_T
3.2	40	125	0	0	0
1.6	340	122	0	0	0

Polymerizations were performed at 5.5 bar of ethylene, 60 °C for 30 min, with 3.3 μ mol of Zr and 1000 equivalents of MAO.

ethylene and 1-octene was performed. If the co-monomer inserts as a hexyl branch, then the support is influencing how the catalyst makes the macromonomers. However, if only linear polyethylene is produced then the active site is sterically hindered by the support. The polymerization trials with 1-octene are shown in Table 5. No branching occurred when 1-octene is added to the reaction. This indicates that the support is hindering the active site, preventing any α -olefins—whether made *in situ* or manually added—into the backbone of the polymers.

Microscopy images of these polymers were obtained and are shown in Fig. 16. PE made from the homogeneous **1** (Fig. 16A and B) show that flakey layers of polymers are formed during polymerization. As these polymers are not melted before microscopy, the images show how the PE forms during polymerization. These polymers form quite differently when compared to the PE produced from the supported catalyst. The ones made by 5@magadiite (C and D) are not flakey at all, the flat surface of the polymer displays several defects. A closer view of the image shows the silica support in white (Fig. 16D). PE from 5@AlPO-kanemite shows a more defective surface but there are some indications of flakey layers within the material (E and F). These images show that the supports drastically influence the fashion in which the polymer forms during polymerization.

These results on polymerization using supported Oct-amido (catalyst **5**) shed some light on the way to control the degree of branching on the PE chain using heterogeneous catalysts. Recent results⁴² on the preparation of polyethylene nanocomposites by constrained geometry catalysts (CGCs) have been obtained by reacting the cocatalyst MAO and catalyst **5** with different 2D supports. Polyethylene nanocomposites were produced with good activities and a plenty of control on the branching content of PE.

3.5. The nature of 2D and 3D structures and tethering catalyst strategies

What sets zirconocenes apart from other catalysts is that the zirconocene unit is able to perform selective carbon–carbon bond-forming reactions due to its ability to stabilize alkynes and alkenes.⁴³ Turning these systems heterogeneous adds the benefits of heterogeneous catalysis like recyclability with the controlled transformations that occur at the single site metal center, provided by the homogeneous system. There are many strategies proposed to generate well-defined heterogeneous

catalysts, not only for zirconocenes but also for metal complexes as Grubbs' ruthenium catalyst,¹⁶ RuCl₃ anchored onto functionalized silica for oxidation of benzylic alcohols,⁴⁴ W, Mo, Re, and Ru organometallic complexes⁴⁵ and so on. The formation of covalent bonds between the support surface and metal complexes is a challenge. For zirconocene complexes as well as for other organometallic complexes, immobilization can be reached by the direct grafting of the complex onto the support and anchoring of the complex *via* a covalent linkage between the support surface and one of the ligands of the complex.^{11,13–21}

Immobilizations *via* non-covalent interactions like ionic interactions or physisorption, for example, are less common due to the leaching aspects. In the case of zirconocenes, when applied for polymerization, regardless the type of anchoring employed, the complexes as well as the zirconium metal are retained in the final polymer chain. Thus, a judicious choice of the supports allows the formation of interesting composites. Moreover, whether the catalyst does not deactivate and is sufficiently stable under the reaction conditions, a good immobilization methodology would be reached.

The presence of the support in the surroundings of the metallocene plays the role of a bulky binder, reflecting in steric and electronic effects of smaller or higher order, that end up influencing the monomer access to the active center and the properties of the final polymer composites.

The catalyst built in close proximity to the surface of a mesoporous solid, like 1@MCM-41 employing the silane strategy shown in the present work, had no activity in the production of olefins. One of the factors related is that the system can be assembled in face-up or face-down configurations due to the proximity to the support surface. An endeavour to reduce such interaction was binding the metal center far from the surface using an alkyl group as a spacer. Thereupon, catalyst **2** was assembled on the surface of a mesoporous material (MCM-48) and the system was active for ethylene polymerization (350 kg of PE per mol Zr per h). However, a bulky organic complex like catalyst 3@MCM-41 can hinder the access of the monomers into the cavity of the support where the active sites are lodged. Besides the hindrance effect, the restricted region forced the zirconium complex to interact with the OH group on the surface of the support. The Cl/Zr molar ratios of 2@MCM-41 and 3@MCM-41 samples are 1.2/1.0 and 1.6/1.0, respectively, which is evidence of the confining effect and possible binding of the zirconium with the surface. In an ideal situation, where no interaction with the surface occurs, the ratio should be 2/1. The monochloride species found for these catalysts forces the metal center to interact with the surface groups of the support. This is not unexpected since the complex has been assembled into the cavity of these mesoporous solids as the data from N₂ isotherms showed by the thickening of their walls after the catalyst construction.

If the inner region of the support where the catalyst is housed can be expanded, as in the case of the layered magadiite, the bending of the organic chain is not extensive and the catalyst performance could be improved. This is what happens

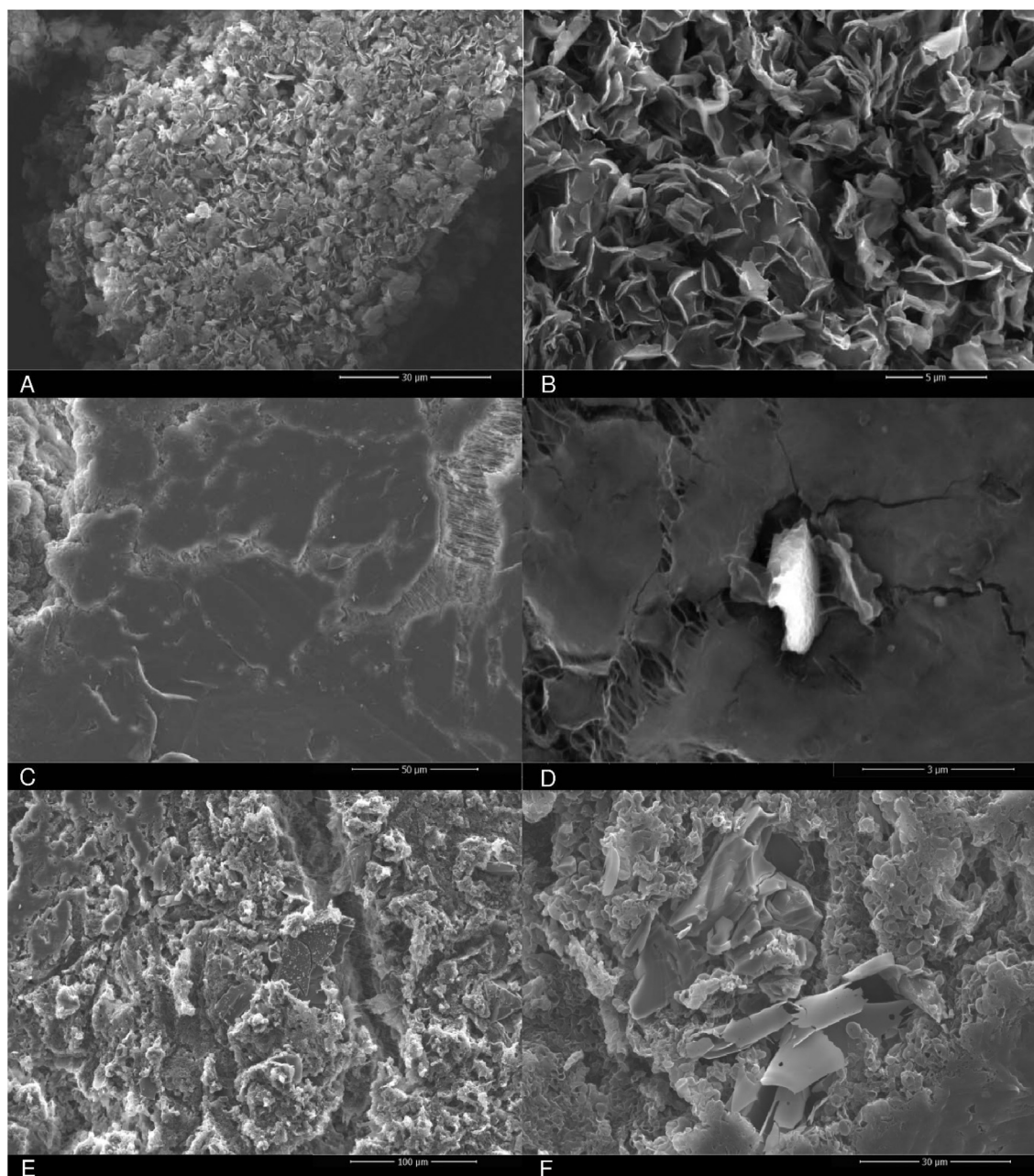


Fig. 16 SEM images of PE. (A) Image and (B) close up image of homogeneous 5. (C) Image and (D) close up image of PE made by 5@magadiite. (E) Image and (F) close up image of PE from 5@AlPO-kanemite.

when **2** is built on the surface of magadiite. The performance of **2**@magadiite on the synthesis of polyethylene almost doubled compared to the same zirconium complex **2**@MCM-48. This clearly is evidence of the role of the bidimensional structure in comparison with the tridimensional one.

For polymerization to occur in the heterogeneous catalyst, the monomers must be able to penetrate into the structure and access the metal sites. Thus, the porosity of the solid structure should aid the polymerization reaction if there is enough room to do so. In the cases studied here, the meso-

porous solids MCM-41 and MCM-48 showed evidence of limited molecular movement within the pores and, in most of the cases, leading to the trapping of the zirconium complexes on the surface. The less constrained environments within a solid structure, like layered supports, open up the possibilities of designing systems and their final products, *e.g.*, when catalyst **5** was supported on two different types of layered supports (magadiite and *n*-alkyl-AlPO-kanemite), the ability to fine tune the guest species in these supports can lead to bimodal PE or to a purely linear HDPE.

4. Conclusions

Primary-amine-functionalized materials have been prepared and used as supports for tethered catalysts. Other strategies tested were the grafting of fluorene and the direct construction on the inorganic surfaces. Direct anchoring of homogeneous catalysts was also performed. From the ethylene polymerization results using methylaluminoxane as the co-catalyst, two main features have to be highlighted when these catalysts are tethered: (i) the site for covalent attachment should be remote from the catalytic site for olefin coordination and insertion. Due to the presence of a flexible $-(\text{CH}_2)_3\text{NH}-$ chain, the metallic center interacts with $-\text{OH}$ on the inorganic surface (confirmed by UV-Vis spectra of the final solids) and access of the ethylene monomers and/or short chains to the Zr^{4+} center is difficult, leading to lower activities and poor-branched PE production. Actually, the activity of 2@magadiite (656 kg of PE per mol Zr per h) whose layers are expandable are expressively higher than the activity of 2@MCM-48 (353 kg of PE per mol Zr per h) and catalyst 3@MCM-41 (30 kg of PE per mol Zr per h) where the catalysts are hindered into the pores. Both catalysts produced HDPE with melting temperatures in the range of 130–135 °C.

Apart from these results, the direct grafting of the fluorene on the support surface led to catalyst 1@MCM-41 which assembles in an undesired face-down conformation with the surface. Once the metal center becomes hindered, it is limited in its conformational freedom on the surface, preventing the monomer coordination and no polymer can be obtained in this case. (ii) The catalyst must be chemically stable and not be cleaved during the catalytic cycle as in the case of catalyst 4, as seen by NMR and UV-Vis right after the Zr addition, and if detached from the surface, it needs to be kept assembled.

Supporting the homogeneous Oct-amido catalyst (5) on inorganic supports affects the active site and changes how the catalyst polymerized ethylene and propylene. Once the catalyst was supported on the layered supports magadiite and AlPO₄kanemite, the active site became sterically hindered and the catalyst could no longer incorporate the α -olefins produced *in situ* into the polymer backbone. This was shown by both an increase in melting temperatures and a lack of branching peaks in carbon NMR.

Conflicts of interest

There are no conflicts to declare.

Acknowledgements

The authors acknowledge the Funding agencies that have supported this work: Conselho Nacional de Desenvolvimento Científico (CNPq, grant number 140737/2013-8) and Coordenação de Aperfeiçoamento de Pessoal de Nível Superior (CAPES, grant number 7266/15-4).

References

- 1 R. Geyer, J. R. Jambeck and K. L. Law, *Sci. Adv.*, 2017, **3**, 25–29.
- 2 M. Stürzel, S. Mihañ and R. Mühlaupt, *Chem. Rev.*, 2016, **116**, 1398–1433.
- 3 M. Jezequel, V. Dufaud, M. J. Ruiz-Garcia, F. Carrillo-Hermosilla, U. Neugebauer, G. P. Niccolai, F. Lefebvre, F. Bayard, J. Corker, S. Fiddy, J. Evans, J. P. Broyer, J. Malinge and J. M. Basset, *J. Am. Chem. Soc.*, 2001, **123**, 3520–3540.
- 4 J. C. W. Chien, *Top. Catal.*, 1999, **7**, 23–36.
- 5 P. C. Lebaron, Z. Wang and T. J. Pinnavaia, *Appl. Clay Sci.*, 1999, **15**, 11–29.
- 6 J. Liu, W.-J. Boo, A. Clearfield and H.-J. Sue, *Mater. Manuf. Processes*, 2006, **21**, 143–151.
- 7 K. Tangjituabun, B. Jongsomjit and P. Praserttham, *Catal. Commun.*, 2009, **10**, 1319–1323.
- 8 W. Kaminsky and C. Strübel, *J. Mol. Catal. A: Chem.*, 1998, **128**, 191–200.
- 9 N. V. Semikolenova and V. A. Zakharov, *Macromol. Chem. Phys.*, 1997, **198**, 2889–2897.
- 10 M. C. Sacchi, D. Zucchi, I. Tritto, P. Locatelli and T. Dall'Occo, *Macromol. Rapid Commun.*, 1995, **16**, 581–590.
- 11 J. R. Severn, J. C. Chadwick, R. Duchateau and N. Friederichs, *Chem. Rev.*, 2005, **105**, 4073–4147.
- 12 B. Y. Lee and J. S. Oh, *Macromolecules*, 2000, **33**, 3194–3195.
- 13 V. Varga, M. Večeřa, R. Gyepes, J. Pinkas, M. Horáček, J. Merna and M. Lamač, *ChemCatChem*, 2017, **9**, 3160–3172.
- 14 J. Pinkas and M. Lamač, *Coord. Chem. Rev.*, 2015, **296**, 45–90.
- 15 V. Varga, M. Horáček, Z. Bastl, J. Merna, I. Císařová, J. Sýkora and J. Pinkas, *Catal. Today*, 2012, **179**, 130–139.
- 16 K. Melis, V. De D., P. Jacobs and F. Verpoort, *J. Mol. Catal. A: Chem.*, 2001, **169**, 47–56.
- 17 M. Kwanten, B. a. M. Carrière, P. J. Grobet and P. a. Jacobs, *Chem. Commun.*, 2003, 1508.
- 18 M. De Bruyn, M. Limbourg, J. Denayer, G. V. Baron, V. Parvulescu, P. J. Grobet, D. E. De Vos and P. A. Jacobs, *Appl. Catal., A*, 2003, **254**, 189–201.
- 19 H. G. Alt, *J. Chem. Soc., Dalton Trans.*, 1999, 1703–1709.
- 20 E. I. Iiskola, S. Timonen, T. T. Pakkanen, O. Härkki, P. Lehmus and J. V. Seppälä, *Macromolecules*, 1997, **30**, 2853–2859.
- 21 M. Benaglia, A. Puglisi and F. Cozzi, *Chem. Rev.*, 2003, **103**, 3401–3429.
- 22 H. O. Pastore, M. Munsignatti, D. R. S. Bittencourt and M. M. Rippel, *Microporous Mesoporous Mater.*, 1999, **32**, 211–228.
- 23 G. B. Superti, E. C. Oliveira, H. O. Pastore, A. Bordo, C. Bisio and L. Marchese, *Chem. Mater.*, 2007, **19**, 4300–4315.
- 24 D. L. Felix, M. Strauss, L. C. Ducati and H. O. Pastore, *Microporous Mesoporous Mater.*, 2009, **120**, 187–194.
- 25 H. I. Meléndez-Ortiz, Y. A. Perera-Mercado, L. A. García-Cerda, J. A. Mercado-Silva and G. Castruita, *Ceram. Int.*, 2014, **40**, 4155–4161.

- 26 H. O. Pastore, M. Munsignatti and A. J. S. Mascarenhas, *Clays Clay Miner.*, 2000, **48**, 224–229.
- 27 L. J. Irwin, J. H. Reibenspies and S. A. Miller, *J. Am. Chem. Soc.*, 2004, **126**, 16716–16717.
- 28 S. A. Miller and J. E. Bercaw, *Organometallics*, 2004, **23**, 1777–1789.
- 29 G. B. Galland, R. F. de Souza, R. S. Mauler and F. F. Nunes, *Macromolecules*, 1999, **32**, 1620–1625.
- 30 L. J. Irwin, J. H. Reibenspies and S. A. Miller, *J. Am. Chem. Soc.*, 2004, **126**, 16716–16717.
- 31 W. Li, H. Chung, C. Daeffler, J. A. Johnson and R. H. Grubbs, *Macromolecules*, 2012, **45**, 9595–9603.
- 32 C. Alonso-Moreno, D. Pérez-Quintanilla, D. Polo-Cerón, S. Prashar, I. Sierra, I. del Hierro and M. Fajardo, *J. Mol. Catal. A: Chem.*, 2009, **304**, 107–116.
- 33 P. I. Ravikovitch and a. V. Neimark, *Langmuir*, 2000, **16**, 2419–2423.
- 34 The dimensions of the organic structures were simulated using the WebMO freeware developed by: J. R. Schmidt and W. F. Polik, WebMO Enterprise, Version 18.0.002e; WebMO LLC: Holland, MI, USA, 2018, available at <http://www.webmo.net> (accessed in 01/08/2018).
- 35 A. Ramanathan, B. Subramaniam, R. Maheswari and U. Hanefeld, *Microporous Mesoporous Mater.*, 2013, **167**, 207–212.
- 36 E. Fernández López, V. Sánchez Escribano, M. Panizza, M. M. Carnasciali and G. Busca, *J. Mater. Chem.*, 2001, **11**, 1891–1897.
- 37 X. Cheng, O. W. Lofthus and P. A. Deck, *J. Mol. Catal. A: Chem.*, 2004, **212**, 121–126.
- 38 B. Marler, U. Oberhagemann, S. Vortmann and H. Gies, *Microporous Mater.*, 1996, **6**, 375–383.
- 39 M. Yadavi, A. Badiei, G. Ziarani and A. Abbasi, *Chem. Pap.*, 2013, **67**, 751–758.
- 40 A. C. dos Ouros, C. Favero, M. O. de Souza, R. F. de Souza and H. O. Pastore, *J. Mol. Catal. A: Chem.*, 2016, **422**, 59–68.
- 41 S. Zakrzewska, A. C. Dos Ouros, N. Schramm, D. Jehnichen, L. Häussler, D. Pospiech, B. Voit, U. Schulze and H. O. Pastore, *Eur. Polym. J.*, 2015, **65**, 238–251.
- 42 H. M. Moura, N. L. Gibbons, S. A. Miller and H. O. Pastore, 2D-Aluminum-Modified Solids as Simultaneous Support and Cocatalyst for In Situ Polymerizations of Olefins. Submitted to Journal of Catalysis (Ref: JCAT-17-1511).
- 43 R. D. Broene and S. L. Buchwald, *Science*, 1993, **261**, 1696–1701.
- 44 S. Sahi and S. Paul, *Green Chem. Lett. Rev.*, 2012, **5**, 343–351.
- 45 H. Balcar and J. Čejka, *Coord. Chem. Rev.*, 2013, **257**, 3107–3124.